Rigorous, Full-Vectorial Source-type Integral Equation Analysis of Circularly Curved Channel Waveguides

Harrie J. M. Bastiaansen, J. Michiel van der Keur, and Hans Blok, *Member, IEEE*

***Abstract*—A source-type integral equation method is presented to determine the propagation constants, the radiation losses, and the electromagnetic field distributions of the discrete ("guided") modes in circularly curved, integrated optical channel waveguides embedded in a homogeneous background. The method can be extended to the case of a multilayered background, e.g. a ridge waveguide. The source-type integral equation forms an eigenvalue problem, where the electric field strength represents the eigenvector. This problem is solved numerically by applying the method of moments. Numerical results are presented for various rectangular channel waveguides situated in a homogeneous embedding and compared with those of other modeling methods.**

I. Introduction

OPTICAL WAVEGUIDES are the basic components of optoelectronic integrated circuits. They interconnect various devices present on a circuit. As such, interconnecting waveguide tracks along which light is guided consist of both straight and curved sections. The sections are either of the ridge waveguide type or of the diffused channel type. For a successful design of these optoelectronic circuits, accurate modeling tools for both straight and curved waveguides are essential. In this paper we focus on a rigorous computation of the properties of the curved waveguide sections, i.e. radiation loss and modal field distributions. In recent approaches to tackle this problem [1], [2] an effective index method for curved waveguides has been most widely used to transform the rather complicated ridge or channel waveguide structure into a curved slab waveguide structure (for an excellent overview see [3]). The approximations made in these approaches show that although good curved waveguide designs have been made, there is still need for a rigorous approach to the problem, particularly when higher-contrast media are going to be used. The formulation of the general 3-dimensional curved waveguide problem in terms of source-type integral equations along the lines followed by Baken [4] and others [5]–[7] provides such a rigorous approach.

Whether a particular modeling approach can be applied succesfully depends on the radius of curvature (in terms of the operating wavelength) and on the contrast between the core of the curved waveguide and its surrounding. Due to their approximations, most earlier approaches are restricted to curved structures with relative large radii of curvature. An extensive discussion on the actual numerical modeling of bent slab waveguides is presented in the book by Vassallo [3, ch. 5]. It shows that little has been published about a full-vectorial analysis of sharply bent waveguides. Apart from the Effective Index Method [1] and the Method of Lines [2], Rozzi has studied the effect of curvature using a "local modes" technique [8], and Oksanen and Lindell [9] have investigated transversely anisotropic, curved waveguides with a variational technique. A beam propagation analysis of bent optical waveguides [10] has been based on the scalar wave equation.

In [11] we used a source-type integral equation analysis to investigate the simplest curved waveguiding structure: the circularly curved, radial inhomogeneous slab waveguide. In the present paper a full-vectorial source-type integral equation analysis of circularly curved channel waveguides with arbitrary cross-section embedded in a homogeneous background is presented. Applying an azimuthal Fourier transform, a source-type integral equation for the electric field strength within the waveguiding region in the azimuthal spectral domain is derived. With an appropriate spatial Fourier transform in the transverse direction, a transverse spectral domain representation for the electric Green's tensor is derived, allowing for an integral equation formulation in which the singular part of the Green's tensor is integrated analytically. The resulting integral equation is subsequently solved with the method of moments. In order to do this efficiently and in a numerically stable manner, special care is needed for the proper choice for the expansion and weighting functions. Numerical results have been obtained for curved channel waveguides with a rectangular cross-section. Results will be discussed and compared with those of other numerical techniques. In this paper we restrict ourselves to channel waveguides embedded in a homogeneous background. However, similar to the source-type integral analysis for straight channel waveguides [6], the formulation can be extended to channel waveguides in a multi-layered background (e.g. a ridge waveguide), providing a powerful modeling tool for the design of optical waveguides. This will be the goal of forthcoming research.

II. Formulation of the Problem

The waveguiding structure we will investigate is the circularly curved channel waveguide embedded in a homogeneous background (Fig. 1). A right-handed cylindrical reference frame $\{O, \underline{i}_x, \underline{i}_\rho, \underline{i}_\varphi\}$ is introduced to specify the position

Manuscript received August 18, 1993; revised March 30, 1994.

H. J. M. Bastiaansen and J. M. van der Keur are with the Dr. Neher Laboratory, PTT Research, 2260 AK Leidschendam, The Netherlands.

H. Blok is with the Department of Electrical Engineering, Delft University of Technology, 2600 GA Delft, The Netherlands.

IEEE Log Number 9407287.

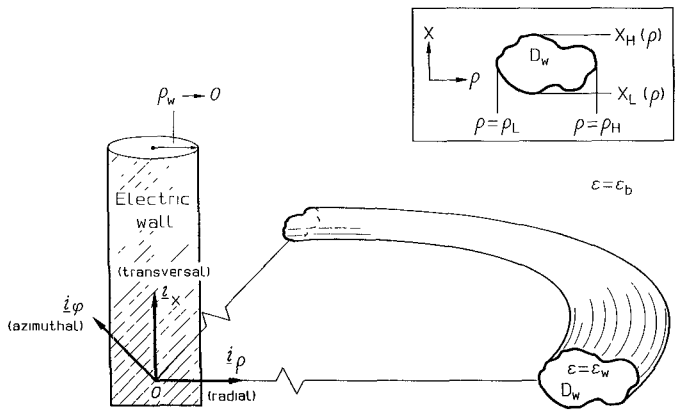

Fig. 1. Configuration of the circular curved channel waveguide in an homogeneous background.

in space. The x-axis coincides with the axis of curvature, the φ-axis is along the center of the channel waveguide, and the ρ-axis points in the radial direction. The background has permittivity ε_b and permeability μ_0. The background exhibits losses and its permittivity is complex and situated in the fourth quadrant of the complex plane:

$$\varepsilon_b = \varepsilon_b' - j\varepsilon_b'', \qquad \varepsilon_b', \varepsilon_b'' > 0. \tag{1}$$

The channel waveguide has arbitrary cross-section D_w with an inhomogeneous permittivity profile $\varepsilon_w(x,\rho)$ and permeability μ_0. The cross-section of the waveguide D_w is described through

$$D_w: \qquad \rho_L < \rho < \rho_H, \qquad x_L(\rho) < x < x_H(\rho). \tag{2}$$

The channel waveguide is circularly curved around the axis $\rho = 0$. The azimuthal φ-direction is assumed to extend to infinity, i.e. no 2π-periodicity of the electromagnetic fields is assumed. As a consequence, the various parts of the curved section have to be insulated from each other's radiation fields. Therefore, a perfectly conducting screen is put around the axis of curvature. In our case, the screen is placed at the origin $\rho_w = 0$.

In the waveguiding structure discrete modes can propagate. These are time-harmonic solutions of the source-free Maxwell equations for which the field profiles show no deformation upon propagation through the structures, i.e. the field profiles are independent of the azimuthal φ-coordinate. For discrete modes propagating in the positive azimuthal direction, the electromagnetic field constituents of angular frequency ω and azimuthal wavenumber k_φ have the form

$$\{\underline{E}, \underline{H}\}(x,\rho,\varphi,t) = \{\underline{\tilde{E}}, \underline{\tilde{H}}\}(x,\rho;k_\varphi)\exp[j(\omega t - k_\varphi \varphi)]. \tag{3}$$

The discrete modes in curved waveguides are discrete in the azimuthal direction, but leaky in nature [11]. The azimuthal wavenumber k_φ is complex valued and situated in the fourth quadrant of the complex plane:

$$k_\varphi = k_\varphi' - jk_\varphi'', \qquad k_\varphi', k_\varphi'' > 0. \tag{4}$$

The complex time factor $\exp[j\omega t]$ is omitted in the remainder of this paper. The field constituents are solutions of Maxwell's equations in the space domain in cylindrical coordinates:

$$-\tilde{\underline{\nabla}} \times \underline{\tilde{H}}(x,\rho;k_\varphi) + j\omega\varepsilon(x,\rho)\underline{\tilde{E}}(x,\rho;k_\varphi) = \underline{0},$$
$$\tilde{\underline{\nabla}} \times \underline{\tilde{E}}(x,\rho;k_\varphi) + j\omega\mu_0\underline{\tilde{H}}(x,\rho;k_\varphi) = \underline{0}, \tag{5}$$

where the space domain nabla-operation $\tilde{\underline{\nabla}}\times$ is defined through

$$\tilde{\underline{\nabla}} \times \underline{\tilde{A}} = \{\frac{1}{\rho}\partial_\rho(\rho\tilde{A}_\varphi) + \frac{jk_\varphi}{\rho}\tilde{A}_\rho\}\underline{i}_x + \{-\frac{jk_\varphi}{\rho}\tilde{A}_x - \partial_x\tilde{A}_\varphi\}\underline{i}_\rho + \{\partial_x\tilde{A}_\rho - \partial_\rho\tilde{A}_x\}\underline{i}_\varphi. \tag{6}$$

Maxwell's equations (5) are a set of six homogeneous coupled partial differential equations. Non-trivial solutions only exist for discrete values of the azimuthal wavenumber k_φ. These solutions are the discrete modes of the curved channel waveguide, the k_φ-values are the propagation constants. In this paper a full-vectorial source-type integral equation method is derived to determine the propagation constants and the amplitude distributiuons of these discrete modes. In [11], the source-type integral method was succesfully applied to the case of circularly curved slab waveguides. In the next section, the source-type integral equation analysis for circularly curved channel waveguides embedded in an homogeneous background is derived. The extension of this method to multilayered backgrounds will be the subject of a subsequent paper.

III. The Source-type Integral Equations

In the source-type integral analysis, the channel waveguide D_w is regarded as a perturbation of its homogeneous embedding through the introduction of an electric contrast source in Maxwell's equations (5):

$$-\tilde{\underline{\nabla}} \times \underline{\tilde{H}}(x,\rho;k_\varphi) + j\omega\varepsilon_b\underline{\tilde{E}}(x,\rho;k_\varphi) = -\underline{\tilde{J}}^c(x,\rho;k_\varphi),$$
$$\tilde{\underline{\nabla}} \times \underline{\tilde{E}}(x,\rho;k_\varphi) + j\omega\mu_0\underline{\tilde{H}}(x,\rho;k_\varphi) = \underline{0}, \tag{7}$$

where $\underline{\tilde{J}}^c$ represents the electric contrast-source density that is defined within the waveguide D_w through

$$\underline{\tilde{J}}^c(x,\rho;k_\varphi) = j\omega\{\varepsilon(x,\rho) - \varepsilon_b\}\underline{\tilde{E}}(x,\rho;k_\varphi) \tag{8}$$

and vanishes everywhere outside D_w.

Integral representations for the solution of (7) can be obtained in several ways. A derivation on the basis of the vector eigenfunction expansion of the dyadic Green's tensor as described for a closely related problem in [12, ch. 2] is possible. Because of its intrinsic simplicity, however, we use the shift-invariance of the homogeneous background in the transversal x-direction in this paper to solve (7) in the transverse Fourier domain. Hitherto, Maxwell's equations in the spatial domain (7) are submitted to the spatial Fourier transformation

$$\tilde{f}(k_x) = \int_{-\infty}^{\infty} f(x)\exp[jk_x x]dx,$$
$$f(x) = \frac{1}{2\pi}\int_{-\infty}^{\infty}\tilde{f}(k_x)\exp[-jk_x x]dk_x, \tag{9}$$

yielding Maxwell's equations in the Fourier transform domain

$$-\tilde{\tilde{\underline{\nabla}}}(k_x;\rho;k_\varphi) \times \underline{\tilde{\tilde{H}}}(k_x;\rho;k_\varphi) + j\omega\varepsilon_b\underline{\tilde{\tilde{E}}}(k_x;\rho;k_\varphi) = -\underline{\tilde{\tilde{J}}}^c(k_x;\rho;k_\varphi),$$
$$\tilde{\tilde{\underline{\nabla}}}(k_x;\rho;k_\varphi) \times \underline{\tilde{\tilde{E}}}(k_x;\rho;k_\varphi) + j\omega\mu_0\underline{\tilde{\tilde{H}}}(k_x;\rho;k_\varphi) = \underline{0}, \tag{10}$$

in which the Fourier transform domain nabla-operation $\underline{\underline{\tilde{\nabla}}}\times$ is defined as

$$\begin{aligned}\underline{\underline{\tilde{\nabla}}}(k_x;\rho;k_\varphi)\times\underline{\tilde{A}} &= \{\frac{1}{\rho}\partial_\rho(\rho\tilde{A}_\varphi)+\frac{jk_\varphi}{\rho}\tilde{A}_\rho\}\underline{i}_x\\ &+\{-\frac{jk_\varphi}{\rho}\tilde{A}_x+jk_x\tilde{A}_\varphi\}\underline{i}_\rho\\ &+\{-jk_x\tilde{A}_\rho-\partial_\rho\tilde{A}_x\}\underline{i}_\varphi, \qquad (11)\end{aligned}$$

and the Fourier transformed electric contrast-source density equals

$$\underline{\tilde{J}}^c(k_x;\rho;k_\varphi)=\int_{x_L(\rho)}^{x_H(\rho)}\underline{J}^c(x,\rho;k_\varphi)\exp[jk_xx]dx. \qquad (12)$$

The meaning of $x_L(\rho)$ and $x_H(\rho)$ is indicated in Fig. 1.

For the solution of Maxwell's equations in the Fourier transform domain (10) a source-type integral representation can be derived. The derivation is based on the global form of Lorentz's reciprocity theorem.

A. Lorentz's Reciprocity Theorem

The local form of Lorentz's reciprocity theorem follows from application of the transverse nabla-operator $\underline{\underline{\tilde{\nabla}}}_t.\underline{\underline{\tilde{F}}}=1/\rho\ \partial_\rho(\rho\underline{\underline{\tilde{F}}}_\rho)$ to the vector

$$\begin{aligned}\underline{\underline{\tilde{F}}} =&\underline{\underline{\tilde{E}}}^A(k_x;\rho;k_\varphi)\times\underline{\underline{\tilde{H}}}^B(-k_x;\rho;-k_\varphi)\\ &-\underline{\underline{\tilde{E}}}^B(-k_x;\rho;-k_\varphi)\times\underline{\underline{\tilde{H}}}^A(k_x;\rho;k_\varphi), \qquad (13)\end{aligned}$$

where the electromagnetic fields $\{\underline{\underline{\tilde{E}}}^A,\underline{\underline{\tilde{H}}}^A,\underline{\tilde{J}}^A\}(k_x;\rho;k_\varphi)$ and $\{\underline{\underline{\tilde{E}}}^B,\underline{\underline{\tilde{H}}}^B,\underline{\tilde{J}}^B\}(k_x;\rho;k_\varphi)$ satisfy the electromagnetic field equations (10) in the same spatial domain. Using the vector relations

$$\begin{aligned}\underline{\underline{\tilde{\nabla}}}_t.(\underline{\underline{\tilde{E}}}^A\times\underline{\underline{\tilde{H}}}^B)&=\underline{\underline{\tilde{H}}}^B.\underline{\underline{\tilde{\nabla}}}(k_x;\rho;k_\varphi)\times\underline{\underline{\tilde{E}}}^A\\ &-\underline{\underline{\tilde{E}}}^A.\underline{\underline{\tilde{\nabla}}}(-k_x;\rho;-k_\varphi)\times\underline{\underline{\tilde{H}}}^B,\\ \underline{\underline{\tilde{\nabla}}}_t.(\underline{\underline{\tilde{E}}}^B\times\underline{\underline{\tilde{H}}}^A)&=\underline{\underline{\tilde{H}}}^A.\underline{\underline{\tilde{\nabla}}}(-k_x;\rho;-k_\varphi)\times\underline{\underline{\tilde{E}}}^B\\ &-\underline{\underline{\tilde{E}}}^B.\underline{\underline{\tilde{\nabla}}}(k_x;\rho;k_\varphi)\times\underline{\underline{\tilde{H}}}^A, \qquad (14)\end{aligned}$$

and Maxwell's equations (10), the local form of Lorentz's reciprocity theorem in the Fourier transform domain becomes

$$\begin{aligned}\underline{\underline{\tilde{\nabla}}}_t\times\{&\underline{\underline{\tilde{E}}}^A(k_x;\rho;k_\varphi)\times\underline{\underline{\tilde{H}}}^B(-k_x;\rho;-k_\varphi)\\ &-\underline{\underline{\tilde{E}}}^B(-k_x;\rho;-k_\varphi)\times\underline{\underline{\tilde{H}}}^A(k_x;\rho;k_\varphi)\}\\ =&\ \underline{\underline{\tilde{E}}}^B(-k_x;\rho;-k_\varphi).\underline{\tilde{J}}^A(k_x;\rho;k_\varphi)\\ &-\underline{\underline{\tilde{E}}}^A(k_x;\rho;k_\varphi).\underline{\tilde{J}}^B(-k_x;\rho;-k_\varphi). \qquad (15)\end{aligned}$$

To transform the local form of the reciprocity theorem into a global one, (15) is substituted into the one-dimensional divergence theorem of Gauss

$$\begin{aligned}\int_{\mathcal{L}}\underline{\underline{\tilde{\nabla}}}_t\times\underline{\underline{\tilde{F}}}(k_x;\rho;k_\varphi)\rho d\rho &= \rho_H\underline{\underline{\tilde{F}}}_\rho(k_x;\rho_H;k_\varphi)\\ &-\rho_L\underline{\underline{\tilde{F}}}_\rho(k_x;\rho_L;k_\varphi), \qquad \mathcal{L}=(\rho_L,\rho_H). \qquad (16)\end{aligned}$$

For vector fields $\rho\underline{\underline{\tilde{F}}}(k_x;\rho;k_z)$ vanishing at the origin $\rho=0$ and at infinity $\rho=\infty$, the right-hand side vanishes. Substitution of the reciprocity theorem in local form (15) yields its global form

$$\begin{aligned}\int_S\{&\underline{\underline{\tilde{E}}}^B(-k_x;\rho;-k_\varphi).\underline{\tilde{J}}^A(k_x;\rho;k_\varphi)\\ &-\underline{\underline{\tilde{E}}}^A(k_x;\rho;k_\varphi).\underline{\tilde{J}}^B(-k_x;\rho;-k_\varphi)\}\rho d\rho=0, \qquad (17)\end{aligned}$$

in which S is an arbitrary ρ-interval enclosing all external electric sources.

B. Source-type Integral Equations in the Fourier Transform Domain

In the reciprocity theorem (17), state "A" is identified with the electromagnetic field distribution $\{\underline{\underline{\tilde{E}}},\underline{\underline{\tilde{H}}},\underline{\tilde{J}}^c\}$ of a discrete mode. Subsequently, state "B" is for $p=x,\rho,\varphi$ identified with the Green's state $\{\underline{\underline{\tilde{E}}}^{G,p},\underline{\underline{\tilde{H}}}^{G,p},(1/\rho')\delta(\rho-\rho')\underline{i}_p\}$ for an electric point-source, situated in $\rho=\rho'$ and oriented in the direction of the unit vector $\underline{i}_p$. Substitution of the electromagnetic fields of state "A" and state "B" in the global form of the reciprocity theorem yields

$$\begin{aligned}\tilde{E}_p(k_x;\rho';k_\varphi)=&\int_{\rho_L}^{\rho_H}\underline{\underline{\tilde{E}}}^{G,p}(-k_x;\rho,\rho';-k_\varphi).\\ &\underline{\tilde{J}}^c(k_x;\rho;k_\varphi)\rho d\rho. \qquad (18)\end{aligned}$$

For the meaning of ρ_L and ρ_H, see Fig. 1. The tensor $\underline{\underline{\tilde{G}}}$ is the electric Green's tensor containing $\underline{\underline{\tilde{E}}}^{G,p}$ as its p-th column:

$$\underline{\underline{\tilde{G}}}_{qp}(-k_x;\rho,\rho';-k_\varphi)=\underline{\underline{\tilde{E}}}_q^{G,p}(-k_x;\rho,\rho';-k_\varphi). \qquad (19)$$

For the electric Green's tensor a reciprocity relation can be obtained by identification of the electromagnetic state $\{\underline{\underline{\tilde{E}}},\underline{\underline{\tilde{H}}},\underline{\tilde{J}}^c\}$ in (18) temporarily with the second Green's state $\{\underline{\underline{\tilde{E}}}^{G,q},\underline{\underline{\tilde{H}}}^{G,q},(1/\rho'')\delta(\rho-\rho'')\underline{i}_q\}$, for $q=x,\rho,\varphi$. This results in

$$\underline{\underline{\tilde{G}}}_{pq}(k_x;\rho',\rho'';k_\varphi)=\underline{\underline{\tilde{G}}}_{qp}(-k_x;\rho'',\rho';-k_\varphi). \qquad (20)$$

Through substitution of the Green's tensor and its reciprocity relation in (18), and redefinition of the variables $\{\rho,\rho'\}$ the source-type integral representation for the electric field solution of Maxwell's equations in the Fourier transform (10) domain is found as:

$$\underline{\underline{\tilde{E}}}(k_x;\rho;k_\varphi)=\int_{\rho_L}^{\rho_H}\underline{\underline{\tilde{G}}}(k_x;\rho,\rho';k_\varphi).\underline{\tilde{J}}^c(k_x;\rho';k_\varphi)\rho'd\rho'. \qquad (21)$$

C. The Green's Tensor

The kernel of the source-type integral equation (21) consists of the electric Green's tensor $\underline{\underline{\tilde{G}}}$ in the Fourier transform domain. To determine the Green's tensor, the Maxwell equations (10) for the point-source problem $\underline{\tilde{J}}^c=(1/\rho')\delta(\rho-\rho')\underline{i}_p$ have to be solved. For $p=x,\rho,\varphi$, the solution $\underline{\underline{\tilde{E}}}^{G,p}$ of (10) is the p-column of the electric Green's tensor.

For $\rho \neq \rho'$ the equations are homogeneous. They consist of four coupled ordinary differential equations, complemented with two algebraic equations. Hence, the general solution contains four independent variables. Following [13, p. 91], the transversal components $\{\tilde{\tilde{E}}_x, \tilde{\tilde{H}}_x\}$ satisfy the scalar wave equation

$$\partial_\rho \partial_\rho \tilde{\tilde{E}}_x + \frac{1}{\rho}\partial_\rho \tilde{\tilde{E}}_x - \frac{k_\varphi^2}{\rho^2}\tilde{\tilde{E}}_x + k_\rho^2 \tilde{\tilde{E}}_x = 0,$$
$$\partial_\rho \partial_\rho \tilde{\tilde{H}}_x + \frac{1}{\rho}\partial_\rho \tilde{\tilde{H}}_x - \frac{k_\varphi^2}{\rho^2}\tilde{\tilde{H}}_x + k_\rho^2 \tilde{\tilde{H}}_x = 0,$$
$$k_\rho = \sqrt{k^2 - k_x^2}, \qquad Im\{k_\rho\} \leq 0. \tag{22}$$

Subsequently, the radial and azimuthal field components $\{\tilde{\tilde{E}}_\rho, \tilde{\tilde{E}}_\varphi, \tilde{\tilde{H}}_\rho, \tilde{\tilde{H}}_\varphi\}$ can be expressed in the transversal components $\{\tilde{\tilde{E}}_x, \tilde{\tilde{H}}_x\}$.

The general solution of the scalar wave equation is a linear combination of the Bessel function $J_{k_\varphi}(k_\rho \rho)$ and Hankel function of the second kind $H^{(2)}_{k_\varphi}(k_\rho \rho)$. Since the field components have to be bounded at $\rho = 0$, the Hankel-function has to be absent in the area $0 \leq \rho < \rho'$. In this region the general solution becomes

$$\{\tilde{\tilde{\underline{E}}}, \tilde{\tilde{\underline{H}}}\}(k_x; \rho; k_\varphi) = \{\tilde{\tilde{\underline{\underline{E}}}}, \tilde{\tilde{\underline{\underline{H}}}}\} J_{k_\varphi}(k_\rho \rho) . \begin{bmatrix} f_E^< \\ f_H^< \end{bmatrix}, \tag{23}$$

with

$$\tilde{\tilde{\underline{\underline{E}}}} = \begin{bmatrix} 1 & 0 \\ \frac{-jk_x\partial_\rho}{k_\rho^2} & -\frac{\omega\mu_0 k_\varphi}{k_\rho^2 \rho} \\ \frac{-k_\varphi k_x}{k_\rho^2 \rho} & \frac{j\omega\mu_0\partial_\rho}{k_\rho^2} \end{bmatrix}, \quad \tilde{\tilde{\underline{\underline{H}}}} = \begin{bmatrix} 0 & 1 \\ \frac{\omega\varepsilon_b k_\varphi}{k_\rho^2 \rho} & -\frac{jk_x\partial_\rho}{k_\rho^2} \\ \frac{-j\omega\varepsilon_b\partial_\rho}{k_\rho^2} & -\frac{k_\varphi k_x}{k_\rho^2 \rho} \end{bmatrix}.$$

The boundary condition of outward travelling, exponential decaying fields at $\rho \to \infty$ requires that the Bessel function is absent in the area $\rho' < \rho < \infty$. The general solution in this region is obtained from (10) through substitution $\{J_{k_\varphi}(k_\rho \rho), f_E^<, f_H^<\} \to \{H^{(2)}_{k_\varphi}(k_\rho \rho), f_E^>, f_H^>\}$.

To determine the constants $\{f_E^<, f_H^<, f_E^>, f_H^>\}$, the general solutions for the regions $0 \leq \rho < \rho'$ and $\rho' < \rho < \infty$ are matched at $\rho = \rho'$. To this end, the radial field components $\tilde{\tilde{E}}_\rho, \tilde{\tilde{H}}_\rho$ are eliminated from (23) with the help of the algebraic relations. The resulting set of four first-order differential equations for the transversal and azimuthal field components is integrated over an infinitesimal small ρ-interval containing the point-source at $\rho = \rho'$. Integration of the Dirac functions gives a finite-size step at $\rho = \rho'$ for the field-components:

$$\begin{bmatrix} \tilde{\tilde{E}}_x^{G,p} \\ \tilde{\tilde{E}}_\varphi^{G,p} \\ \tilde{\tilde{H}}_x^{G,p} \\ \tilde{\tilde{H}}_\varphi^{G,p} \end{bmatrix} (\rho' + 0) - \begin{bmatrix} \tilde{\tilde{E}}_x^{G,p} \\ \tilde{\tilde{E}}_\varphi^{G,p} \\ \tilde{\tilde{H}}_x^{G,p} \\ \tilde{\tilde{H}}_\varphi^{G,p} \end{bmatrix} (\rho' - 0) = \begin{bmatrix} \frac{k_x}{\omega\varepsilon_b \rho'} \delta_{p\rho} \\ \frac{k_\varphi}{\omega\varepsilon_b \rho'^2} \delta_{p\rho} \\ -\frac{1}{\rho'}\delta_{p\varphi} \\ \frac{1}{\rho'}\delta_{px} \end{bmatrix}, \tag{24}$$

in which δ_{pq} is the Kronecker symbol. Its value is 1 if p and q are equal and 0 otherwise. With the general solution (23) in the regions $0 \leq \rho < \rho'$ and $\rho' < \rho < \infty$ four linear relations for the four constants $\{f_E^<, f_H^<, f_E^>, f_H^>\}$ result, providing a unique solution. Subsequently, the p-column of the electric Green's tensor follows as the electric field in the general solution (23). The Green's tensor becomes

$$\tilde{\tilde{\underline{\underline{G}}}}(k_x; \rho, \rho'; k_\varphi) = \tilde{\tilde{\underline{\underline{G}}}}^r(k_x; \rho, \rho'; k_\varphi) + \tilde{\tilde{\underline{\underline{G}}}}^s(k_x; \rho, \rho'; k_\varphi), \tag{25}$$

with the equations shown at the bottom of the page.

D. Source-type Integral Equations in the Spatial Domain

In (25), the Green's tensor is split in a regular part (superscript "r") and a singular part (superscript "s"). The singular part takes the Dirac function in the radial electric field component into account. The regular part of the Green's tensor is finite at $\rho = \rho'$. Hence, integration of the regular part of the Green's tensor can be done straightforwardly. The singular part is only present in the $\rho\rho$ component of the Green's tensor and contains the Dirac function $\delta(\rho - \rho')$. Analytic integration of the singular part is possible. Substitution of the electric Green's tensor (25) in the integral representation (21) and analytic integration of the singular part yields

$$\tilde{\tilde{\underline{E}}}(k_x; \rho; k_\varphi) - \frac{j}{\omega\varepsilon_b}\tilde{\tilde{\underline{J}}}^c(k_x; \rho; k_\varphi).\underline{i}_\rho = \int_{\rho_L}^{\rho_H} \tilde{\tilde{\underline{\underline{G}}}}^r(k_x; \rho, \rho'; k_\varphi).\tilde{\tilde{\underline{J}}}^c(k_x; \rho'; k_\varphi)\rho' d\rho'. \tag{26}$$

$$\tilde{\tilde{\underline{\underline{G}}}}^s = -\frac{1}{j\omega\varepsilon_b\rho'}\delta(\rho - \rho')\begin{bmatrix} 0 & 0 & 0 \\ 0 & 1 & 0 \\ 0 & 0 & 0 \end{bmatrix},$$

$$\tilde{\tilde{\underline{\underline{G}}}}^r = \frac{\pi}{2\omega\varepsilon_b}\hat{\underline{\underline{G}}}^r . H^{(2)}_{k_\varphi}(k_\rho \rho_>) J_{k_\varphi}(k_\rho \rho_<), \qquad \rho_< = \min\{\rho, \rho'\}, \qquad \rho_> = \max\{\rho, \rho'\},$$

$$\hat{\underline{\underline{G}}}^r = \begin{bmatrix} -k_\rho^2 & -jk_x\partial_{\rho'} & \frac{k_x k_\varphi}{\rho'} \\ jk_x\partial_\rho & -\frac{k_x^2}{k_\rho^2}\partial_\rho\partial_{\rho'} & \frac{-jk_x^2 k_\varphi}{k_\rho^2 \rho'}\partial_\rho \\ \frac{k_x k_\varphi}{\rho} & \frac{jk_x^2 k_\varphi}{k_\rho^2 \rho}\partial_{\rho'} & \frac{-k_x^2 k_\varphi^2}{k_\rho^2 \rho\rho'} \end{bmatrix} + \begin{bmatrix} 0 & 0 & 0 \\ 0 & \frac{-k^2 k_\varphi^2}{k_\rho^2 \rho\rho'} & \frac{-jk^2 k_\varphi}{k_\rho^2 \rho}\partial_{\rho'} \\ 0 & \frac{jk^2 k_\varphi}{k_\rho^2 \rho'}\partial_\rho & -\frac{k^2}{k_\rho^2}\partial_\rho\partial_{\rho'} \end{bmatrix}.$$

Through direct substitution it can straightforwardly be checked that (26) indeed represents the solution of (10). The representation of the solution of Maxwell's equation in the spatial domain (7) follows after application of the inverse Fourier transformation. Furthermore, the electric contrast source (8) and its Fourier representation (12) are substituted:

$$\underline{\tilde{E}}(x;\rho;k_\varphi) - \frac{j}{\omega\varepsilon_b}\underline{\tilde{J}}^c(x;\rho;k_\varphi).\underline{i}_\rho = \frac{j\omega}{2\pi}.\int_{-\infty}^{\infty}\int\int_{D_w}\underline{\underline{\tilde{G}}}^r(k_x;\rho,\rho';k_\varphi).\{\varepsilon_w(x',\rho')-\varepsilon_b\}\underline{\tilde{E}}(x;\rho';k_\varphi)\exp[jk_x(x'-x)]\rho'dx'd\rho'dk_x. \quad (27)$$

For observation points (x,ρ) inside the channel waveguide D_w, the electric field appears at both the left and right hand side. Hence, (27) constitutes a homogeneous Fredholm integral equation of the second kind. A nontrivial solution exists only for those discrete values k_φ that are propagation constants of discrete modes. The corresponding solution represents the electric field distribution of the discrete mode. The magnetic field can be found by taking the curl of the electric field strength.

The integral equation can be solved with the method of moments, as will be outlined in Section IV.

IV. Numerical Implementation

The source-type integral equation analysis applies to channel curved waveguide structures with an arbitrary cross-section. In the numerical computations, however, we restrict ourselves to channel waveguides with a rectangular cross-section D_w:

$$D_w: \qquad -\frac{h}{2} \le x \le \frac{h}{2}, \qquad \rho_L \le \rho \le \rho_H.$$

The channel waveguide and background are assumed homogeneous (with permittivity ε_w and ε_b, respectively) and loss-free: $\varepsilon_w, \varepsilon_b \in R$. The numerical implementation plays an important role in the succesful application of the source-type integral equation method. Hence, an extensive discussion of its numerical aspects is given in this section.

In order to find the nontrivial solutions of the source-type integral equation, the method of moments is applied [14]. The electric field $\underline{\tilde{E}}(x,\rho)$ is expanded into a series of expansion functions $f_{pq}(x,\rho)$.

$$\underline{\tilde{E}}(x,\rho) = \sum_{p,q=1,1}^{P,Q}\underline{\tilde{E}}_{pq}f_{pq}(x,\rho), \qquad (x,\rho)\epsilon D_w. \quad (28)$$

Subsequently, a weighting procedure with weighting functions $w_{mn}(x,\rho)$ is applied over the cross-section of the waveguide. Both the expansion functions and the weighting functions are chosen separable in an x-dependent and a ρ-dependent part

$$f_{pq}(x,\rho) = f_p^\rho(\rho)f_q^x(x),$$
$$w_{mn}(x,\rho) = w_m^\rho(\rho)w_n^x(x),$$
$$m,p \in \{1,...,P\}, n,q \in \{1,...,Q\}. \quad (29)$$

Substitution of the expansion of the electric field (28) in the source-type integral equation (27) and application of the weighting procedure yields a set of $3*P*Q$ homogeneous linear algebraic equations for $3*P*Q$ components of the expansion vectors $\underline{\tilde{E}}_{pq}$, shown in (30) at the bottom of the page, in which

$$L_{nq}^x = \int_{-h/2}^{h/2} w_n^x(x).f_q^x(x)dx, \quad (31)$$

$$L_{mp}^\rho = \int_{\rho_L}^{\rho_H} w_m^\rho(\rho).f_p^\rho(\rho)d\rho, \quad (32)$$

$$R_{nq}^x(k_x)7pc = \int_{-h/2}^{h/2}\int_{-h/2}^{h/2} \times \exp[jk_x(x'-x)]w_n^x(x).f_q^x(x')dx'dx, \quad (33)$$

$$\underline{\underline{R}}_{mp}^\rho(k_x;k_\varphi) = \int_{\rho_L}^{\rho_H}\int_{\rho_L}^{\rho_H}\underline{\underline{\tilde{G}}}^r(k_x;\rho,\rho';k_\varphi)w_m^\rho(\rho) f_p^\rho(\rho')\rho'd\rho'd\rho. \quad (34)$$

The discrete form of the source-type integral equations constitutes a system of $3*P*Q$ homogeneous linear equations. This system can be represented as

$$\mathbf{A}(k_\varphi).\mathbf{E} = \mathbf{0}, \quad (35)$$

in which $\mathbf{A}(k_\varphi)$ is the system's matrix. A nontrivial solution exists only if its determinant is equal to zero. The values of k_φ for which this happens are the propagation constants of the discrete modes. The vector $\mathbf{E}$ contains the individual expansion vectors $\underline{\tilde{E}}_{pq}$ of the electric field distribution of the discrete mode. The zero-determinant condition is the resonance condition for the source-type integral method:

$$\det\{\mathbf{A}(k_\varphi)\} = 0. \quad (36)$$

The numerical procedure used to determine the zeros of the resonance condition (36) in the complex k_φ-plane, is the method as presented by Delves and Lyness [15]. It is based on numerical integration of the Cauchy integrals over a contour enclosing the zeros. The propagation constants of a hybrid Transversal Electric (TE) and its corresonding Transversal Magnetic (TM) counterpart are pair-wise positioned closely together in the complex k_φ-plane. Both propagation constants are computed at the same time. After the propagation constants

$$\sum_{p,q=1,1}^{P,Q} L_{mp}^\rho L_{nq}^x \begin{bmatrix} 1 & 0 & 0 \\ 0 & \frac{\varepsilon_w}{\varepsilon_b} & 0 \\ 0 & 0 & 1 \end{bmatrix}.\underline{\tilde{E}}_{pq} = \frac{j\omega\{\varepsilon_w-\varepsilon_b\}}{2\pi}\sum_{p,q=1,1}^{P,Q}\int_{-\infty}^{\infty}\underline{\underline{R}}_{mp}^\rho(k_x;k_\varphi)R_{nq}^x(k_x)dk_x\underline{\tilde{E}}_{pq},$$

$$m\epsilon\{1,...,P\}, n\epsilon\{1,...,Q\}, \quad (30)$$

k_φ of the discrete modes have been determined, the electric field inside the channel follows from the expansion (28) with the expansion vectors $\underline{\tilde{E}}_{pq}$, which in turn are contained in the eigenvector $\underline{\mathbf{E}}$ of the system's matrix $\mathbf{A}(k_\varphi)$.

To determine the coefficients of the system's matrix, a specific choice for the expansion and weighting functions has to be made, taking into account that the inverse Fourier transformations in (30) have to be implemented. As this is in general a very CPU-time consuming activity, the choice of the expansion functions and weighting functions is done such that these inverse Fourier transformations can be done efficiently and in a numerically stable manner.

The integrand of the inverse Fourier transformation is the product of the tensorial part $\underline{\underline{R}}^{\rho}_{mp}(k_x;k_\varphi)$ and the scalar part $R^x_{nq}(k_x)$. The tensorial part depends on the propagation constant k_φ, whereas the scalar part is not. The infinite integration interval $k_x\epsilon(-\infty,\infty)$ is chopped off to $k_x\epsilon(-C,C)$ and subsequently partitioned into a set of subintervals (A_j,B_j), $j\epsilon\{1,...,J\}$. Each subinterval is normalized to $(-1,1)$ through the introduction of the normalized integration variable $\bar{k}_x = -1+2\dfrac{k_x-A_j}{B_j-A_j}$. Expansion of $\underline{\underline{R}}^{\rho}_{mp}(k_x(\bar{k}_x);k_\varphi)$ into a series of Chebychev polynomials $T_k(\bar{k}_x)$ yields

$$\int_{-\infty}^{\infty}\underline{\underline{R}}^{\rho}_{mp}(k_x;k_\varphi)R^x_{nq}(k_x)dk_x \simeq \sum_{j=1}^{J}\frac{B_j-A_j}{2}\sum_{k=1}^{K}\underline{\underline{R}}^{\rho}_{mp,k}(k_\varphi)\int_{-1}^{1}R^x_{nq}(\bar{k}_x)T_k(\bar{k}_x)d\bar{k}_x. \tag{37}$$

The integrations in (37) are only dependent on the transversal discretization parameters $n,q\epsilon\{1,...Q\}$, the interval number $j\epsilon\{1,...J\}$, and the Chebychev polynomial number $k\epsilon\{1,...K\}$. They are computed numerically and the results are stored. At this point, the evaluation of (37) for specific values of the radial discretization number $m,p\epsilon\{1,...P\}$ and propagation constant k_φ is merely an expansion of the function $\underline{\underline{R}}^{\rho}_{mp}(\bar{k}_x;k_\varphi)$ into a series of Chebychev polynomials and summation of the integrals over the Chebychev polynomials which were already computed. Hence, an extremely efficient algorithm for computing the inverse Fourier transformation is obtained.

In order for this strategy to work in a numerically stable manner, a proper choice for the expansion and weighting functions is required. The boundary C of the integration interval should take the same value for all combinations m,p *epsilon* $\{1,...P\}$ and for all values k_φ. A proper value of C is chosen by defining the radial expansion functions $f^{\rho}_{p}(\rho)$ over the entire width of the channel waveguide, such that all integrands decay as $O(|k_x|^{-\alpha})$, $|k_x|\to\infty$. To minimize the integration length C, the value of α is maximized. By taking the transversal weighting functions $w^x_n(x)$ different from the Dirac function (i.e. no point-matching), $R^x_{nq}(k_x)$ decays as $O(|k_x|^{-2})$, $|k_x|\to\infty$ and the value $\alpha=2$ is guaranteed. With respect to these considerations, we make the following choice for the expansion and weighting functions. In the radial direction we take expansion functions closely related to the cubic B-spline ($f^{\rho}_{p}=B_p$, see [16, p. 199]). The weighting functions are Dirac functions (point-matching, $w^{\rho}_{m}=\delta_m$). In the transversal direction, triangle functions are used as expansion functions ($f^{x}_{q}=\Lambda_q$) and pulse functions as weighting functions ($w^{x}_{n}=\Pi_n$). These expansion and weighting functions are defined through (38), shown at the bottom of the page. For these expansion and weighting functions the spatial integrations in the radial direction (31)–(33) are performed analytically, whereas the spatial integration in the radial direction (34) is performed numerically using a 16-point Gaussian integration rule. These numerical integrations require the Bessel functions $J_{k_\varphi}(k_\rho\rho)$ and $H^{(2)}_{k_\varphi}(k_\rho\rho)$ to be computed for varying values of k_ρ and ρ. The order of the Bessel function is large. The arguments range over the negative imaginary axis and part of the positive real axis. High accuracy for the Bessel function is required. Therefore, in the regions where the order and argument are of the same order of magnitude a numerical implementation of the Bessel functions based on Airy functions [17] is used, with asymptotic expansions listed in [18]. The asymptotic expansions for the Bessel functions are those of Olver [19], [20]. In all other regions the Debye expansion for the Bessel functions is used.

V. Numerical Results

To validate the theory developed in the previous sections and to verify the correctness of the numerical implementation, the source-type integral equation method (STIM) is applied

$$B_p(\rho)=\frac{1}{2}+\frac{1}{8(\Delta\rho)^3}\begin{cases}(\rho-\rho_{p-2})^3 & \text{if} \quad \rho_{p-2}\le\rho\le\rho_{p-1},\\ -3(\rho-\rho_{p-1})^3+3\Delta\rho(\rho-\rho_{p-1})^2+ & \\ +3(\Delta\rho)^2(\rho-\rho_{p-1})+(\Delta\rho)^3 & \text{if} \quad \rho_{p-1}\le\rho\le\rho_{p},\\ -3(\rho_{p+1}-\rho)^3+3\Delta\rho(\rho_{p+1}-\rho)^2+ & \\ +3(\Delta\rho)^2(\rho_{p+1}-\rho)+(\Delta\rho)^3 & \text{if} \quad \rho_{p}\le\rho\le\rho_{p+1},\\ (\rho_{p+2}-\rho)^3 & \text{if} \quad \rho_{p+1}\le\rho\le\rho_{p+2},\\ 0 & \text{else,}\end{cases}$$

$$\delta_m(\rho)=\delta(\rho-\bar{\rho}_m),$$

$$\Lambda_q(x)=\begin{cases}1-\dfrac{|x-x_q|}{\Delta x} & \text{if} \quad -\Delta x\le|x-x_q|\le\Delta x,\\ 0 & \text{else,}\end{cases}$$

$$\Pi_n(x)=\begin{cases}1 & \text{if} \quad -\frac{1}{2}\Delta x\le|x-x_q|\le\frac{1}{2}\Delta x,\\ 0 & \text{else.}\end{cases} \tag{38}$$

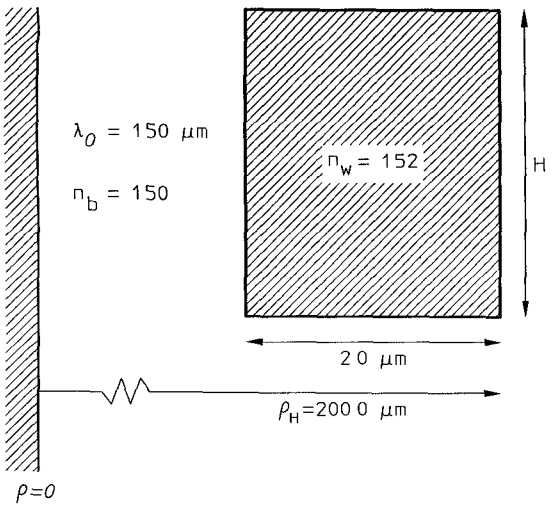

Fig. 2. Curved channel waveguide configuration converging to a curved slab for $H \rightarrow \infty$.

to compute the fundamental hybrid modes of a low-contrast configuration; the configuration of Fig. 2. A curved rectangular channel waveguide with refractive index $n_w = 1.52$ is embedded in a homogeneous background with refractive index $n_b = 1.50$. The width W of the waveguide equals 2.0 μm, whereas its height H is variable. The outer radius of curvature ρ_H equals 800.0 μm. The waveguiding structure is operated at the free-space wavelength $\lambda_0 = 1.5$ μm. The source-type integral equation method is employed with a horizontal discretization number $P = 14$ and a vertical discretization number $Q = 6$, yielding a square system's matrix with dimension $3 * P * Q = 252$. For this discretization each evaluation of a pair of propagation constants typically requires 1 hour of CPU-time on a VAX 6620 computer system.

As the height H tends to infinity, the channel waveguide configuration transforms into a slab waveguide configuration. For the curved slab waveguide numerous numerical methods to compute the propagation constants of the discrete modes are available [11]. In agreement with common convention, the complex propagation constant k_φ of these modes is represented through an effective refractive index term N_{eff} and a radiation loss term L_{rad}, related through

$$N_{eff} = \mathrm{Re}\{k_\varphi\}/(k_0 \rho_H),$$
$$L_{rad} = -10 \cdot \pi \cdot \mathrm{Im}\{k_\varphi\}/\ln(10), \qquad [\mathrm{dB}/(90°)]. \tag{39}$$

The effective refractive index is a measure for the phase velocity of the mode, the radiation loss describes the amount of power radiating away from the channel.

In Fig. 3 radiation loss of the fundamental hybrid modes TE_{00} and TM_{00} of the curved channel waveguide is given as a function of the height H. The curves for $H = \infty$ correspond to the curved slab waveguide. It seems that the radiation losses for the fundamental modes tend to those of the corresponding slab waveguide structure. This ensures the correctness of both the theory and its numerical implementation.

The second configuration we will consider is that of Fig. 4. Again, a rectangular channel waveguide with refractive index $n_w = 1.52$ is embedded in a homogeneous background with

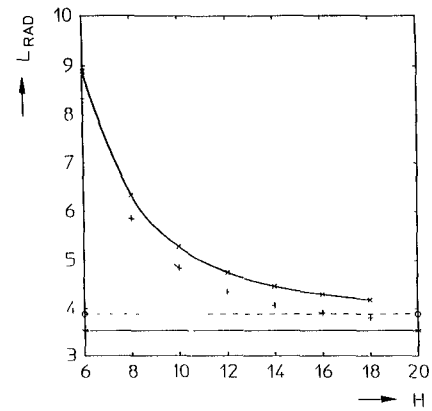

Fig. 3. Radiation loss versus height H of the channel waveguide.

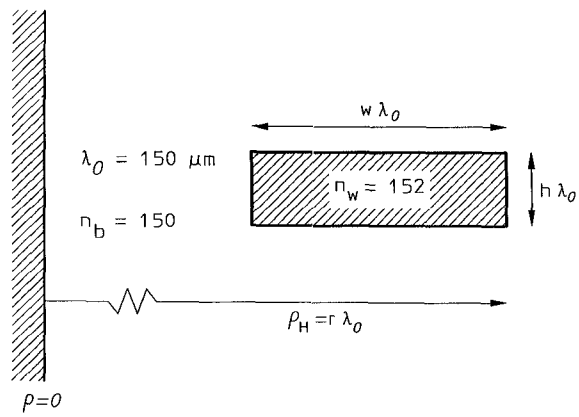

Fig. 4. Curved channel waveguide configuration with varying radius of curvature.

refractive index $n_b = 1.50$. Its width W and height H are expressed in terms of the operating free-space wavelength λ_0: $W = w.\lambda_0$, $H = h.\lambda_0$. Likewise, the outer radius of curvature ρ_H is expressed in terms of λ_0: $\rho_H = r.\lambda_0$. The value r is variable whereas w and h are fixed: $w = 4.0$, $h = 2.0$. For r tending to infinity, the curved channel waveguide structure transforms gradually into a straight one. For the operating free-space wavelength $\lambda_0 = 1.5\mu$m, Table I shows both the effective refracative indices and the radiation losses of the fundamental modes for varying radii of curvature. The results are obtained with discretization $P = 10$ and $Q = 5$. The radiation losses for the fundamental TE-mode are graphically represented in Fig. 5.

For comparison, numerical results for the same configuration as obtained with two other numerical methods have also been included:

1) EIM: In the commonly used effective index method (EIM) the curved channel waveguide structure is replaced by an equivalent curved planar waveguide structure: In the guiding layer the refractive index is equal to the effective refractive index of the inner region $\rho_L \leq \rho \leq \rho_H$ of the channel waveguide structure. The effective index of the regions $\rho < \rho_L$ and $\rho > \rho_H$ is equal to n_b. Numerous numerical techniques for the determination of the propagation constants of the discrete modes of the curved planar waveguide structure exist, cf. [11]

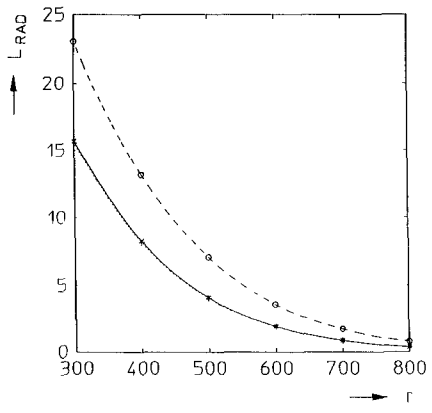

Fig. 5. Radiation loss versus radius of curvature for the TE_{00} mode. Comparison of the source-type integral method, the effective index method, and the method of lines.

2) MoL: In the vectorial version of the Method of Lines (MoL) as presented by Pascher and Pregla [2], a separable solution of the vectorial Maxwell's equation for the curved channel waveguide structure is constructed: in the transversal x-direction a finite difference scheme is applied, whereas in the radial ρ-direction the equations are analytically solved.

For this low-contrast example, Table I shows a remarkable agreement between the numerical results for the propagation properties of the source-type integral equation method and the method of lines. This could be expected as both methods are vectorial and tackle the 3-dimensional configuration. Furthermore, the method of lines is known to be very accurate for low-contrast examples. The numerical results of the effective index method, however, strongly differ from those of the other two methods. This can be ascribed to the reduction of the 3-dimensional configuration to the 2-dimensional one. Our results clearly show that application of the effective index method to curved channel waveguide structures should be done with great care.

The source type-integral equation analysis as presented in this paper is full-vectorial; field-plots of both the transversal component $\tilde{E}_x$ the radial component $\tilde{E}_\rho$ and the azimuthal component $\tilde{E}_\varphi$ can be obtained. Fig. 6(a) shows the intensity plot of the fundamental TE_{00} mode for the radius of curvature equal to $\rho_H = 400\lambda_0$. The shift of the electric field profile towards the outer boundary ρ_H of the channel waveguide is clearly visible. The electric field intensity at the inner boundary ρ_L is negligible. Contour plots of the individual electric field components are shown in Fig. 6(b)–(d). For practical reasons the components of the electric field strength are only computed in the waveguiding domain D_w. Extension to the domain outside D_w is straightforward, but time consuming.

VI. Conclusion

A source-type integral equation analysis has been presented for curved channel waveguides with arbitrary cross-section embedded in a homogeneous background. The analysis is full-vectorial and mathematically rigorous. Numerical results for low-contrast curved rectangular waveguides have been presented and compared with those obtained by the method of lines. The differences in computed propagation losses of the

TABLE I
N_{eff} AND L_{rad} OF THE FUNDAMENTAL MODES VERSUS THE RADIUS OF CURVATURE $\rho_H = r.\lambda_0$ FOR THE CONFIGURATION OF FIG 4: (a) TE-POLARIZATION AND (b) TM-POLARIZATION

	TE_{00}					
	N_{eff}			L_{rad}		
r	STIM	MoL	EIM	STIM	MoL	EIM
800	1.5068269	1.5068216	1.5071128	0.3689	0.3635	0.7837
700	1.5064572	1.5064507	1.5067771	0.8541	0.8421	1.7131
600	1.5059981	1.5059887	1.5063663	1.9097	1.8844	3.5774
500	1.5054095	1.5053956	1.5058465	4.0816	4.0317	7.0747
400	1.5046160	1.5045934	1.5051494	8.2558	8.1663	13.172
300	1.5034476	1.5033661	1.5041183	15.694	15.549	23.047

(a)

	TM_{00}					
	N_{eff}			L_{rad}		
r	STIM	MoL	EIM	STIM	MoL	EIM
800	1.5067611	1.5067598	1.5070402	0.3958	0.3887	0.8393
700	1.5063941	1.5063911	1.5067067	0.9054	0.8901	1.8111
600	1.5059382	1.5059322	1.5062986	2.0003	1.9692	3.7348
500	1.5053538	1.5053433	1.5057817	4.2246	4.1659	7.2986
400	1.5045658	1.5045465	1.5050878	8.4483	8.3468	13.442
300	1.5034044	1.5033661	1.5040591	15.890	15.731	23.290

(b)

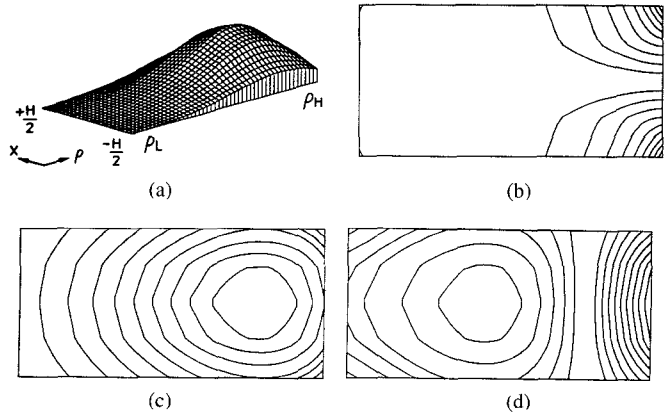

Fig. 6. The fundamental TE_{00} mode at $\rho_H = 400\lambda_0$: (a) intensity, (b) E_x-component, (c) E_ρ-component, and (d) E_φ-component. The lines in the contour-plots are positioned with 10% intensity-steps.

guided modes between these techniques is marginal. However, the numerical result from the commonly used Effective Index Method, in which one dimension of the waveguide structure is eliminated, differ strongly from the other two methods, which take all dimensions into account. Extension of the numerical implementation of the source-type integral method to nonrectangular waveguides is possible, but may require a new choice of expansion and weighting functions.

The forthcoming research will be concenterated on the extension of the source-type integral method to curved channel waveguides embedded in a multi-layered background, as they normally occur in integrated optical applications. For this aim, a formalism similar to the one used in the source-type integral analysis of straight waveguides [6] will be applied. Furthermore, high-contrast channel waveguide configurations will be considered.

ACKNOWLEDGMENT

The authors wish to thank Dr. W. Pascher and Prof. R. Pregla from the Fernuniversität Hagen for providing them with the numerical results of the Method of Lines. Furthermore, the accurate numerical implementation of the Bessel functions by Dr. E.C.M. Pennings is gratefully acknowledged.

REFERENCES

[1] E.C.M. Pennings, "Bends in optical ridge waveguide, modeling and experiments," Ph.D. thesis, University of Technology, Delft, Netherlands, June 1990

[2] W. Pascher and R. Pregla, "Analysis of curved optical waveguides by the vectorial method of lines," in *Proc. IOOC-ECOC 1991*, Apr. 1991, pp. 237–240.

[3] C. Vassallo, *Optical Waveguide Concepts*. Amsterdam: Elsevier Science, 1991.

[4] N. H. G. Baken M. B. J. Diemeer, J. M. van Splunter, and H. Blok, "Computational modeling of diffused channel waveguides using a domain-integral equation," *J. Lightwave Technol.* , vol. 8, no. 4, pp. 576–586, 1990

[5] E. W. Kolk, N. H. G. Baken, and H. Blok, "Domain-integral equation analysis of integrated-optical channel and ridge waveguides in stratified media," *IEEE Trans. Microwave Theory Tech.*, vol. MTT-38, no. 1, pp. 78–85, Jan. 1990

[6] H. J. M. Bastiaansen, N. H. G. Baken, and H. Blok, "Domain-integral analysis of channel waveguides in anisotropic multi-layered media," *IEEE Trans. Microwave Theory Tech.*, vol. MTT-40, no. 10, pp. 1918–1926, Oct. 1992

[7] N. H. G. Baken, "Computational modeling of integrated-optical waveguides," Ph.D. thesis, Drukkerij Plantijn, Rotterdam, 1990.

[8] T. Rozzi, G. C. F. Chiaraluce, R. de Leo, and R. F. Ormondroyd, "Finite curvature and corrugations in dielectric ridge waveguides," *IEEE Trans. Microwave Theory Tech.*, vol. MTT-36, no. 1, pp. 68–79, 1988

[9] M.I. Oksanen and I.V. Lindell Lindell, "Transversely anisotropic curved optical fibers: variational analsysis of a nonstandard eigenproblem," *IEEE Trans. Microwave Theory Tech.*, vol. MTT-37, no. 1, pp. 51–62, 1989.

[10] J. Saijonmaa and D. Yevick, "Beam-propagation analysis of loss in bent optical waveguides and fibers," *J. Opt. Soc. Am.*, vol. 73, no. 12, pp. 1785–1791, Dec. 1983.

[11] H. J. M. Bastiaansen, M. J. van der Keur, and H. Blok, "Rigorously modelling short bent, graded index dielectric slab waveguides," *IEEE Trans. Microwave Theory Tech.*,vol. 41, no. 11, pp. 1972–1980, 1993

[12] R. E. Collin, *Field Theory of Guided Waves*, 2nd ed. New York: IEEE Press, 1991.

[13] L. Lewin, D.C. Chang, and E.F. Kuester, *Electromagnetic Waves and Curved Structures—IEE Electromagnetic Waves Series 2*, J.R. Wait *et al.*, Eds. Stevenage: Peter Peregrinus, 1977.

[14] R. F. Harrington, "The method of moments in electromagnetics," *J Electromag. Waves and Appl.*, vol. 1, no. 3, pp. 181–200, 1987.

[15] L. M. Delves and J. N. Lyness, "A numerical method for locating the zeros of an analytic function," *Math. Comput.*, vol. 21, pp. 543–560, 1967.

[16] T. Hopkins and C. Phillips, *Numerical Methods in Practice, Using the NAG Library*. Norwell, MA: Addison-Wesley, 1988.

[17] E. G. Neumann and W. Richter, "Sharp bends with low losses in dielectric optical waveguides," *Appl. Opt.*, vol. 22, no. 7, pp. 1016–1022, 1983.

[18] M. Abramowitz and I. A. Stegun, *Handbook of Mathematical Functions*. New York: Dover, 1965.

[19] F. W. J. Olver, "Some new asymptotic expansions for *Bessel* functions of large order," in *Proc. Cambridge Philos. Soc.*, 1952, vol. 48, pp. 414–427.

[20] F. W. J. Olver, "The asymptotic expansion of *Bessel* functions of large order," *Phil. Trans. Royal Soc. London*, vol. A247, pp. 328–368, 1954.

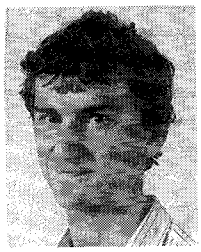

Harrie J. M. Bastiaansen was born in Tilburg, the Netherlands, on May 10, 1965. He received his M.Sc. degree in mathematics, *cum laude*, from the Eindhoven University of Technology in 1988, having specialized in the mechanics of rigid bodies.

In 1989, he became researcher at the PTT Dr. Neher Laboratories, Leidschendam, The Netherlands. At first, his interest was in the guided wave characteristics of straight channel waveguides. At present, he is doing a Ph.D. thesis on the subject of guided wave optics in bent channel waveguides.

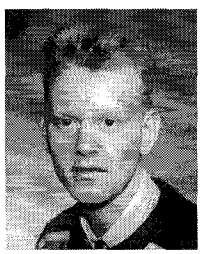

J. Michiel van der Keur was born in Gouda, The Netherlands, on March 16, 1970. He graduated, *cum laude*, in electrical engineering from the Delft University of Technology, where he received the M.Sc. degree in 1993. At present, he is Ph.D. student at the Laboratory of Electromagnetic Research, Delft University of Technology.

During his studies he worked on a Beam Propagation Method at the Centre National d'Etudes des Télécommunications, Lannion, France. He did his master's thesis on rigorous full-vectorial source-type integral equation analysis of circularly curved channel waveguides at the PTT Dr. Neher Laboratories, Leidschendam, The Netherlands. His current research interest is in the field of 3D-BPM-type methods.

Hans Blok (M'87) was born in Rotterdam, The Netherlands, on April 14, 1935. He received a degree in electrical engineering from the Polytechnical School of Rotterdam in 1956. Het then received the B.Sc. and M.Sc. degrees in electrical engineering and the Ph.D. degree in technical sciences, all from the Delft University of Technology, in 1961,1963, and 1970 respectively.

Since 1968, he has been a member of the scientific staff of the Laboratory of Electromagnetic Research at the Delft University of Technology. During these years, he has carried out research and lectured in the areas of signal processing, wave propagation, and scattering problems. During the academic year 1970–1971, he was a Royal Society Research Fellow in the Department of Electronics of the University of Southampton, U.K., where he was involved in experimental and theoretical research on lasers and nonlinear optics. In 1972 he was appointed associate professor at the Delft University of Technology, and in 1980 he was named professor. From 1980 to 1982 he was Dean of the Faculty of Electrical Engineering. During the academic year 1983-1984 he was visiting scientist at Sclumberger-Doll Research, Ridgefield, CT. At present, his main research interest is in guided wave optics and inverse scattering problems.